

INELASTIC SEISMIC RESPONSE OF BRIDGE STRUCTURES SUPPORTED ON EXTENDED PILE SHAFTS

Tara C. HUTCHINSON

*Graduate Student, Department of Civil & Environmental Engineering,
University of California, Davis, California 95616*

Christina J. CURRAS

*Assistant Professor, Department of Civil & Environmental Engineering,
University of Wisconsin, Platteville, WI 53818*

Ross W. BOULANGER, Y.-H. CHAI, and I. M. IDRIS

*Associate Professor, Associate Professor, and Professor, respectively,
Department of Civil & Environmental Engineering,
University of California, Davis, California 95616*

ABSTRACT

The seismic response of bridge and viaduct structures supported on extended cast-in-drilled-hole (CIDH) pile shafts was studied using nonlinear static and dynamic numerical analyses. Results are presented for the effects that near-fault ground motions and variable lateral soil resistance have on system performance. Dynamic analysis results were compared with a force reduction – displacement ductility ($R-\mu-T$) relation and an alternative mean spectral displacement approach. The results suggest that the mean spectral displacement approach has potential for reducing the uncertainty in predicting inelastic displacement demands for these types of structures during near-fault ground motions.

Keywords: bridges, dynamic response, extended pile shafts, inelastic displacement, near-fault ground motions, piles, pushover analysis, soil-structure interaction.

INTRODUCTION

Near-fault ground motions with strong velocity pulses can subject bridge and viaduct structures to very large displacement and ductility demands. For bridge and viaduct structures supported on extended cast-in-drilled-hole (CIDH) pile shafts, plastic hinging in the pile shaft can develop below the ground surface. Residual deformations in these types of structures after an earthquake are an important concern, and may be increased by the presence of strong, uni-directional pulses in the ground motion. The magnitude of inelastic deformation demands in the structure will depend on the ground motion characteristics (including the amplitude, period and shape of any large pulses), the lateral strength and period of the structure, and the hysteretic characteristics of the yielding elements (structural and soil). The seismic performance of these structures will be inherently coupled to the subsurface soil conditions through their influence on site response, foundation stiffness, and energy dissipation.

The damaging effects that near-fault motions have on structures were first observed by Bertero et al. (1978) with their analysis of the Olive View Hospital following the 1971 San Fernando earthquake. It was concluded that inelastic response could not be predicted with reasonable accuracy using methods that modify elastic response spectra. More recently, in evaluating the sensitivity of bridge structures to near-fault motions, Mahin and Hachem (1998) performed dynamic analyses of SDOF systems with details representative of bridge columns and identified trends relating the displacement demands to the fundamental period of the structure and the

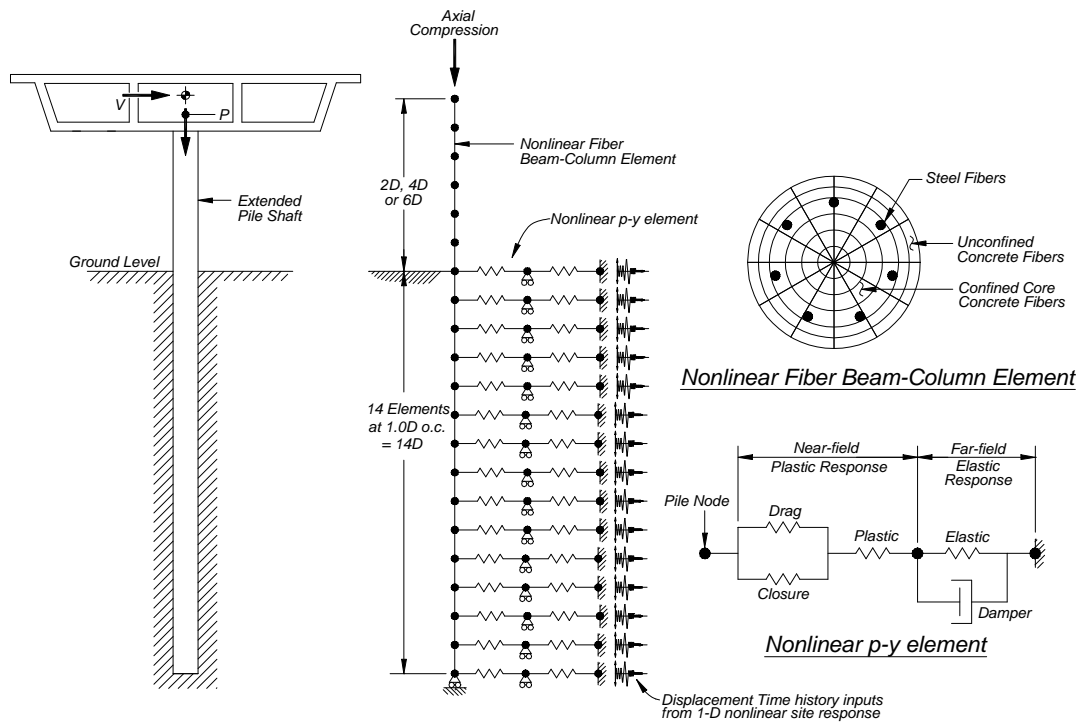


Figure 1. General schematic of the finite element model for the dynamic BNWF analyses using the nonlinear fiber beam-column element and the nonlinear p-y element.

predominant period of the pulse. Regression analysis of their results indicated that for intermediate and long-period structures current practice using the equal displacement principle provided reasonable estimates of inelastic displacement demands. However, they noted the inaccuracy of using current spectral-based techniques for shorter-period structures. Baez and Miranda (2000), using mean values of 82 near-fault ground motions also concluded that for structures with periods less than about 1.3 seconds, inelastic demands were under-estimated using current spectral-based techniques.

This paper describes results from a numerical study of the seismic performance of bridge and viaduct structures supported on extended, large-diameter, CIDH pile shafts. The study included consideration of ground motion characteristics, site response, lateral soil resistance, structural parameters (including geometric nonlinearity), and performance measures. The nonlinear dynamic analyses used a beam on nonlinear Winkler foundation (BNWF) framework to model the soil-pile interaction, nonlinear fiber beam-column elements to model the reinforced concrete sections, and one-dimensional site response analyses for the free-field soil profile response (Fig. 1). The analyses were limited to the transverse response of a single bent. Inelastic displacement demands resulting from the nonlinear dynamic finite element (FE) analyses were compared with displacement demands predicted using nonlinear static methods. Results presented herein focus on how the ground motion characteristics and variability in lateral soil resistance can affect the overall system performance. An alternative design approach that estimates the inelastic demand using the mean elastic spectral displacement between two spectral periods is suggested and shows good promise in minimizing the error associated with predicting inelastic displacements for these types of structures during near-fault motions.

DYNAMIC FINITE ELEMENT ANALYSES

A dynamic BNWF analysis method, as shown in Fig. 1, was used to model the soil-pile interaction. The structural system was modeled using the finite element analysis platform FEAP (Taylor 1998). The CIDH pile and its above-ground extension are modeled using a flexibility-based “fiber” beam-column element from the FEDEAS element library (Filippou 1999). Force resultants in the element are obtained by integrating the fiber

stresses over its cross-section, assuming plane sections remain plane. A modified Kent-Park (1971) model was used to represent the concrete cyclic behavior, and a modified Menegotto-Pinto (1973) model was used to represent the reinforcing steel cyclic behavior. Spacone et al. (1996) describe the slight modifications made to these models. Pile nodes below ground are connected to horizontal p-y elements representing the lateral soil resistance. The nonlinear p-y elements, which account for gapping effects and radiation damping, are described in Boulanger et al. (1999). Parameters for the p-y elements were based on common design procedures used in US practice (details in Curras 2000). Horizontal free-field soil motions obtained from one-dimensional site response calculations were input to the free-field ends of all p-y elements. The site response analyses used the equivalent-linear program SHAKE96 (Schnabel et al. 1972, Idriss and Sun 1991).

Rock Outcrop Motions

A range of earthquake motions with different frequency contents, intensities, durations and permanent displacements were used as rock outcrop motions in this study. Six of these 12 motions, as listed in Table 1, are associated with near-fault recordings and have a strong long-period pulse. Peaks in the elastic (5% damped) response spectra (acceleration and velocity) were used to define a dominant pulse period T_p for each motion. The T_p values ranged from 1.1 to 3.2 s for these near-fault motions. Also note that the near-fault motions recorded during the Taiwan and Turkey earthquakes had large permanent displacements. Of the six “other motions” listed in Table 1, the two synthetic motions each have a particularly long-duration t_d of about 36 s (based on 5-95% cumulative Arias intensity, Trifunac and Brady 1975). For each motion, the peak rock outcrop acceleration (a_{max}) was scaled to produce several intensities for use in the site response analyses, which are described in the following section. Elastic acceleration response spectra, normalized by peak ground acceleration, are shown in Fig. 2 for each of the twelve motions listed in Table 1. Noticeable differences in spectral content for the near-fault motions are seen between periods of 2 and 5 seconds.

Table 1. Earthquake motions used in this study.

Earthquake name & Location of recording	Year	M_w	Channel	a_{max} (g)	v_{max} (m/s)	d_{max} (m)	t_d (s)	T_p (s)	Scaled a_{max} in analyses (g)
(a) Near-fault motions									
San Fernando, Pacoima Dam ¹	1971	6.6	S16°E	0.67	0.956	0.507	7	1.1	0.5, 0.7
Landers, Lucerne	1992	7.5	Transverse	0.71	0.372	0.174	13	1.2	0.3, 0.5, 0.7, 0.9
Northridge, Sylmar	1994	6.8	0°	0.84	1.288	0.304	5	1.4	0.7, 0.9
Chi-Chi Taiwan, Station 068	1999	7.1	East-West	0.51	2.807	7.076	12	2.5	0.3, 0.5
Chi-Chi Taiwan, Station 075	1999	7.1	East-West	0.33	1.163	1.715	27	2.1	0.3, 0.5
Turkey, Yarımcı Petkim	1999	7.1	Transverse	0.32	0.878	1.451	29 ²	3.2	0.3, 0.5, 0.7
(b) Other motions									
Synthetic #1 (Seed and Idriss)	1969	8.0	--	0.5	0.46	0.17	36	N/A	0.5, 0.7
Chile, Valparaiso	1985	8.1	160°	0.41	0.27	0.074	19	N/A	0.3, 0.5, 0.7
Loma Prieta, Gilroy #1	1989	7.1	0°	0.44	0.318	0.107	7	N/A	0.3, 0.5, 0.7
Loma Prieta, Santa Cruz	1989	7.1	0°	0.44	0.217	0.104	9	N/A	0.5, 0.7
Northridge, VA Hospital	1994	6.7	36°	0.94	0.754	0.358	8	N/A	0.7, 0.9
Synthetic #2 (Bay Bridge)	1999	7.5	--	0.52	0.841	0.456	36	N/A	0.3, 0.5, 0.7

¹ Filtering by Page et al. (1972) and topographical modifications by Boore (1973).

² Duration was determined using the 5-95% cumulative Arias intensity from the first event added with the 5-95% cumulative Arias intensity from the second event that immediately followed the first.

Soil Profile and Site Response

A baseline soil profile for this parameter study was modeled after the Gilroy 2 site in California. This site was considered to be a reasonable example of where extended large-diameter CIDH piles might be constructed to support a bridge structure. This site was also characterized extensively by EPRI (1993), including shear wave

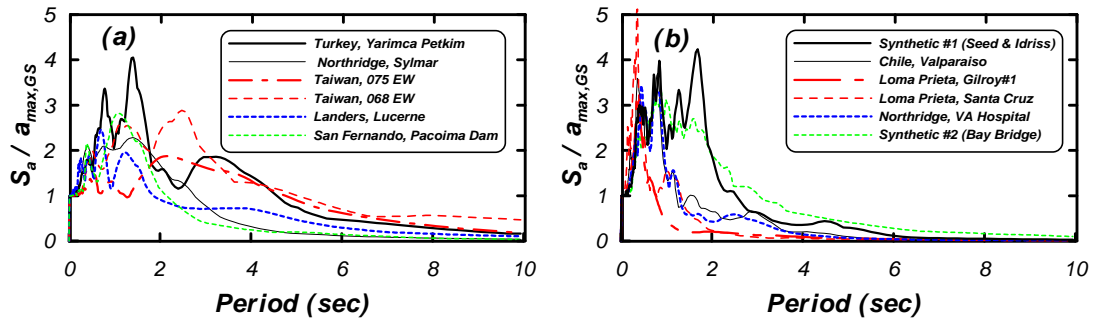


Figure 2. Elastic acceleration response spectra (5% damping) normalized by the peak ground surface acceleration: (a) Near-fault motions, (b) Other motions used in this study.

velocity profiles and cyclic laboratory testing of field samples. The shear wave velocity ranged from 200 to 500 m/s in the upper 30 m, as shown by the profile in Fig. 3. Normalized shear modulus (G/G_{max}) and damping relations for the site response analyses were based on the laboratory test data. The site response for the scaled Synthetic #2 (Bay Bridge) outcrop motions is summarized in Fig. 4. The surface response in terms of spectral acceleration shows the gradual lengthening of the dominant period as the intensity increases, as would be expected due to the larger shear strains and corresponding decrease in secant shear modulus.

Structural Systems

Twelve different bridge structures supported on large-diameter extended CIDH pile shafts were modeled. It is assumed that the transverse response of the bridge structure may be characterized by the response of a single bent, as would be the case for a regular bridge with coherent ground shaking applied to all bents. The extended pile shafts have an above-ground cross-section that is slightly smaller than their below-ground cross-section, in accordance with standard construction detailing. These structures had above-ground heights L_a of 2D, 4D, and 6D, where D (below-ground pile diameter) was taken as both $D = 1.5$ m and $D = 3.0$ m. The embedded pile length was set as 14D for each case based on providing reasonable axial load carrying capacities. Two different axial loads were used in the study, $0.05 \cdot f'_c \cdot A_g$ and $0.1 \cdot f'_c \cdot A_g$, where f'_c = unconfined compressive strength of the concrete, and A_g = gross area of the pile shaft. A concrete compressive strength of $f'_c = 27.6$ MPa was used for both the pile and the above-ground extension. Although concrete strengths may be different for the pile and the

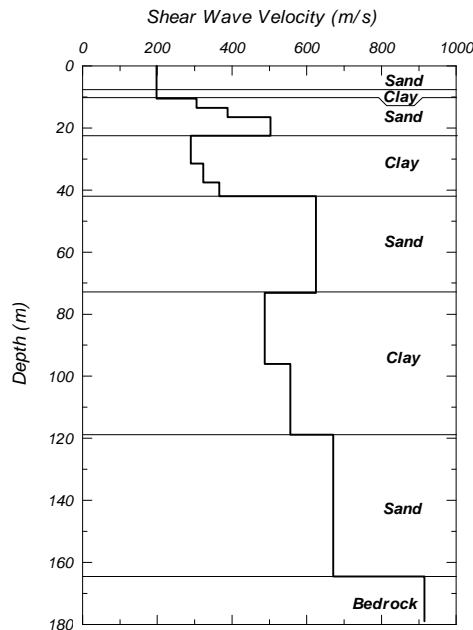


Figure 3. Shear wave velocity profile for baseline site.

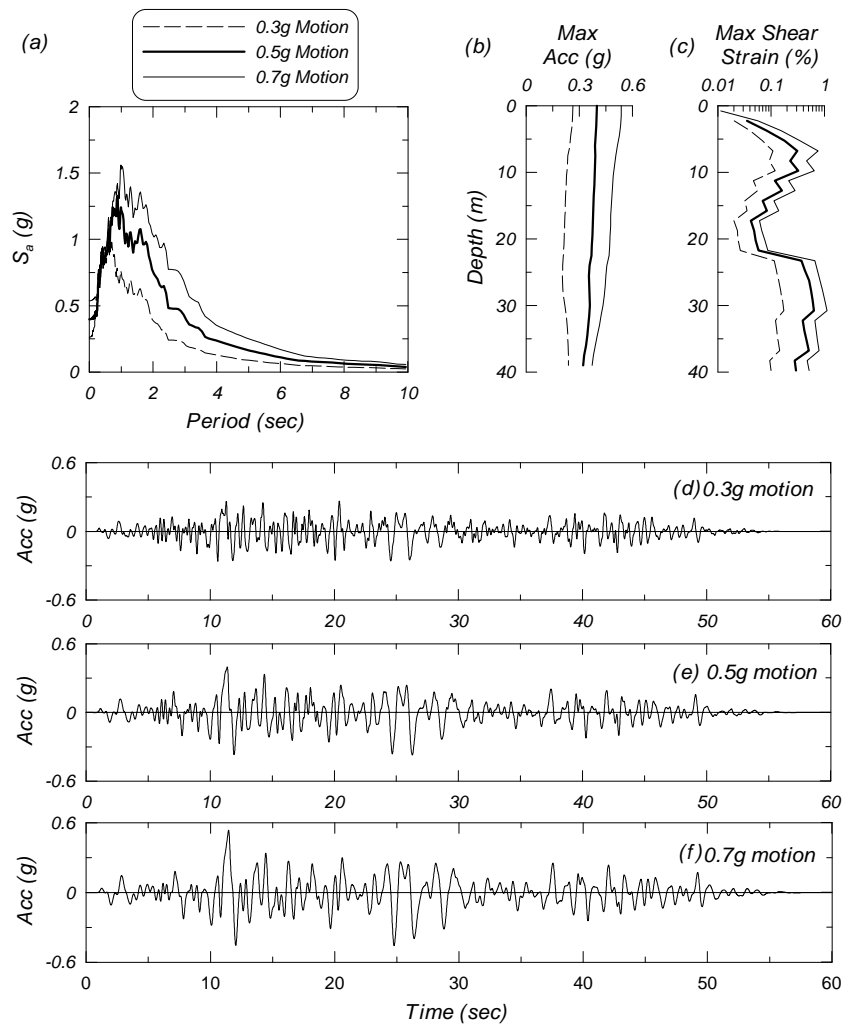


Figure 4. Site response for Synthetic #2 motion: (a) acceleration response spectra (5% damping) at the ground surface, (b) maximum acceleration vs. depth, (c) maximum shear strain vs. depth, (d) surface acceleration history for 0.3g outcrop motion, (e) surface acceleration history for 0.5g outcrop motion, (f) surface acceleration history for 0.7g outcrop motion.

above-ground extension, and actual concrete compressive strengths may be greater than the assumed f'_c value, the resulting lateral stiffness and strength of the pile is not very sensitive to the value of f'_c . Longitudinal and confining reinforcement ratios were about 1%, with nominal yield strengths of $f_y = 414$ MPa. A longitudinal reinforcement ratio of 1% represents the lower end of the longitudinal reinforcement ratios used in practice, however, the objective of this study was to investigate the severity of the inelastic demands on bridge structures with low lateral strength when subjected to ground motions with long-period characteristics. For the level of axial loads imposed on the pile-extension, the amount of confining steel is compatible with current practice (ATC-32 1996).

DYNAMIC ANALYSES RESULTS

The dynamic response of these structures was evaluated in terms of response spectra; time histories and maximum values of superstructure acceleration, inertial force (mass times acceleration), velocity, and displacement; residual displacement of the superstructure; global and local ductility demands; and bending moment distribution in the pile and plastic hinge depth.

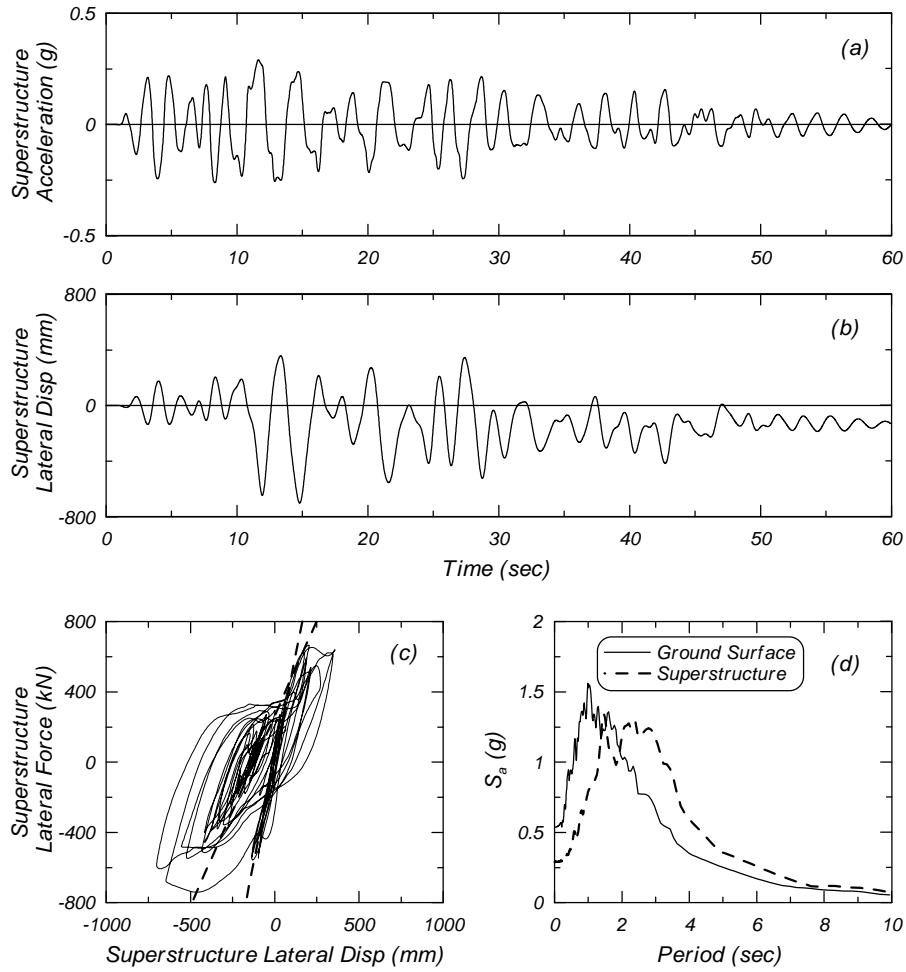


Figure 5. Response of baseline structure with 1.5-m-diameter pile shaft and 4D above-ground height to the Synthetic #2 outcrop motion with $a_{max}=0.7g$: (a) superstructure acceleration, (b) superstructure displacement, (c) superstructure lateral force-displacement response, and (d) elastic acceleration response spectra with 5% damping.

Response quantities are shown in Fig. 5 for one baseline structure and motion – the 1.5-m diameter CIDH pile shaft with an above-ground height of 4D, axial load of $0.05 \cdot f_c' A_g$, subjected to the Synthetic #2 outcrop motion with a scaled a_{max} of 0.7g. The superstructure horizontal acceleration and displacement time histories are shown in parts (a) and (b), respectively, where the acceleration is absolute and the displacement is relative to the pile tip. The maximum displacement of this system is $\Delta_{max} = 700$ mm, which, when divided by the elasto-plastic (EP) yield displacement of $\Delta_y = 170$ mm, gives a global displacement ductility of $\mu_\Delta = 4.1$. The elasto-plastic yield displacement Δ_y was obtained from a nonlinear static pushover analysis of the bridge structure using the same FE model that was used for the dynamic analyses. Note that the displacement time history in Fig. 5(b) also shows a residual displacement at the end of shaking that is 20% of the maximum displacement. The magnitude of residual displacement is important for the serviceability of the structure and will be discussed later in the paper.

The lateral force-displacement time history of the superstructure is shown in Fig. 5(c), where the force is the horizontal acceleration times the superstructure's mass. Of interest is the change in the structure's lateral stiffness caused by the earthquake. The steeper dashed line in Fig. 5(c) corresponds to the initial elastic stiffness (estimated at first-yield of the pile section), whereas the less-steep dashed line corresponds to the lateral stiffness of the system at the end of the ground motion. The structure's lateral stiffness is smaller after the earthquake due to damage in the pile section and degradation in the lateral soil resistance.

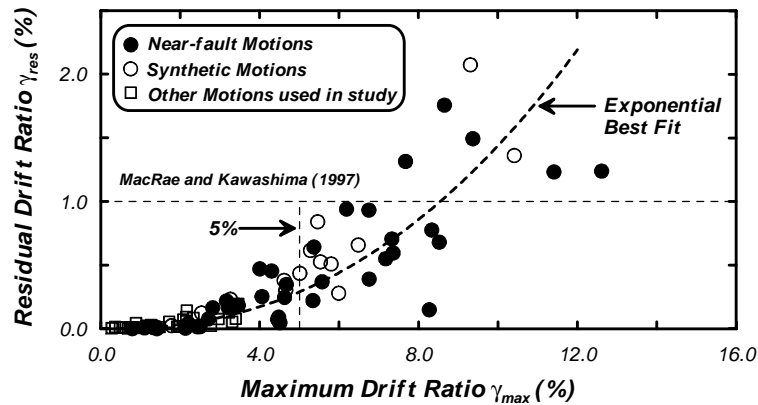


Figure 6. Residual drift ratio γ_{res} as a function of the maximum drift ratio γ_{max} in the superstructure (3.0-m diameter pile shafts with P-D effects).

Elastic acceleration response spectra for the superstructure and ground surface motions are shown in Fig. 5(d). The greatest amplification of motion from the ground surface to the superstructure occurs at a period of about 3 s, which is larger than the equivalent elastic period of the structure ($T_e=1.6$ s) due to the inelastic response of the system.

Maximum and Residual Drift Ratios

For near-fault ground motions, the inelastic response of bridge structures tends to be associated with a biased response in one direction resulting in a large permanent displacement and rotation. The biased lateral response of the structure is often worsened by the combined effect of high axial load, low lateral strength, and increased flexibility due to soil compliance, which collectively increase the importance of geometric nonlinearities or “P- Δ effects.” The recent Japanese experience from the 1995 Hanshin Earthquake indicated that large residual deformations, particularly the residual rotation at the ground level, may render the structure unserviceable or even irreparable after the earthquake (MacRae and Kawashima, 1997). In this study, the permanent or residual drift ratio γ_{res} , defined as the slope (from vertical) of the above-ground pile extension after the earthquake, is used to quantify the magnitude of the permanent deformation in the bridge structure.

Residual drift ratios γ_{res} would reasonably be expected to correlate with the maximum drift ratio γ_{max} , which is defined as the slope of the above-ground pile extension at its peak displacement response. Fig. 6 shows the residual drift ratio γ_{res} versus the maximum drift ratio γ_{max} in the structures supported on 3.0-m diameter pile shafts, with an axial load of $0.05 \cdot f_c' A_g$, and subjected to the motions listed in Table 1. These analyses included P- Δ effects. The residual drift ratio γ_{res} generally increases with the maximum drift ratio γ_{max} , and although there is considerable scatter in Fig. 6, the increase appears to be exponential. Very large maximum drift ratios (greater than 8%) were calculated for some of the bridge structures as a result of their low lateral strength relative to the ground motion demands. A maximum drift ratio of $\gamma_{max} = 5\%$ is indicated in Fig. 6 as a likely maximum drift ratio that may be expected in bridge structures designed with a lateral strength and stiffness compatible with the intensity of the ground motion. For maximum drift ratios of $\gamma_{max} < 5\%$, residual drift ratios are small, generally less than 0.5%. A serviceability residual drift ratio of $\gamma_{res} = 1\%$, as suggested by MacRae and Kawashima (1997), has also been plotted in Fig. 6 for comparison. It is interesting to note that the larger residual drift ratios ($\gamma_{res} > 1\%$) in Fig. 6 were associated with the near-fault and long-duration synthetic ground motions, indicating that these ground motions may be very damaging from a serviceability perspective. Several analyses indicated that the structure would collapse under the near-fault Taiwan and Turkey ground motions, and these results could not be plotted on Fig. 6. It is also worth noting that serviceability drift ratio limits have not been prescribed in current US bridge seismic design codes.

P-D Effects

The influence of P- Δ effects on the seismic response of these structures, particularly when subjected to an intense near-fault ground motion, was also studied. Fig. 7(a) compares the dynamic response of a structure with

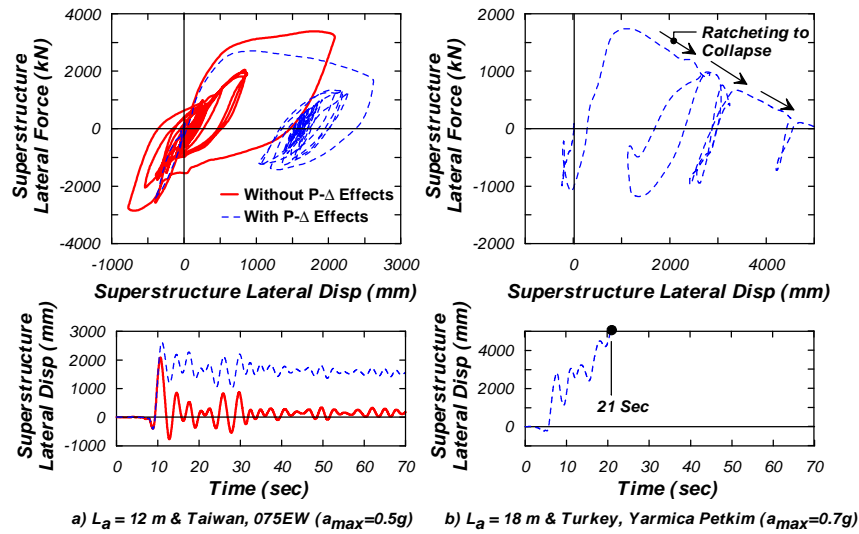


Figure 7. Lateral inertial force-displacement response at the superstructure and lateral displacement time history illustrating sensitivity of inelastic response to P-D effects.

and without P- Δ effects. The structure had a pile diameter of 3.0 m, an above-ground height $L_a = 12$ m, and an axial load of $0.05 \cdot f_c' A_g$. The structure with P- Δ effects experiences a single large displacement excursion to a displacement ductility of $\mu_\Delta = 9.6$ at time $t = 11$ seconds with only limited yielding in the reverse direction during subsequent shaking. The large displacement demand resulted in a large residual drift ratio of $\gamma_{res} = 10.6\%$. In contrast, the same structure analyzed without P- Δ effects experiences a slightly lower displacement ductility demand of $\mu_\Delta = 7.6$ and a much smaller residual drift ratio of $\gamma_{res} = 1.2\%$.

Fig. 7(b) illustrates an extreme case where the analysis that included P- Δ effects indicated that the structure would collapse at time $t = 21$ s. The structure had a pile diameter of 3.0 m, an above-ground height of 18 m, and an axial load of $0.05 \cdot f_c' A_g$. In this case, a single large displacement excursion led to instability of the structure. The same structure without P- Δ effects also experienced large inelastic displacements (to a maximum displacement ductility of $\mu_\Delta = 7.5$), but did not collapse.

These examples illustrate that P- Δ effects are particularly important for this type of structure when the earthquake ground motions produce large inelastic displacements. However, including P- Δ effects for structures that experienced ductility demands μ_Δ less than 3.0 (with axial loads of $0.05 \cdot f_c' A_g$) caused less than a 30% increase in the residual drift ratio for 70% of the cases analyzed and less than a 30% increase in the maximum drift ratio for 90% of the cases analyzed.

Effects of p-y Parameter Variation on Seismic Response

The sensitivity of the dynamic response of these types of structures to the lateral soil resistance, or p-y parameters, was evaluated for a subset of structures and ground motions. This parametric study considered the effects p-y parameter variations have on various performance measures for the structure, including peak superstructure displacement and local curvature ductility in the pile. However, prior to describing the results of this parametric study, general sources of uncertainty in p-y parameters and a reasonable range of variation that might be encountered in practice are discussed.

Predicting the lateral loading response of piles is affected by numerous sources of uncertainty, including the following factors.

- Limitations in our ability to accurately characterize the soil profile, including the extent and continuity of individual soil layers.
- Limitations in our methods for estimating soil parameters, which often include empirical relations, SPT or CPT correlations, or laboratory testing of samples.

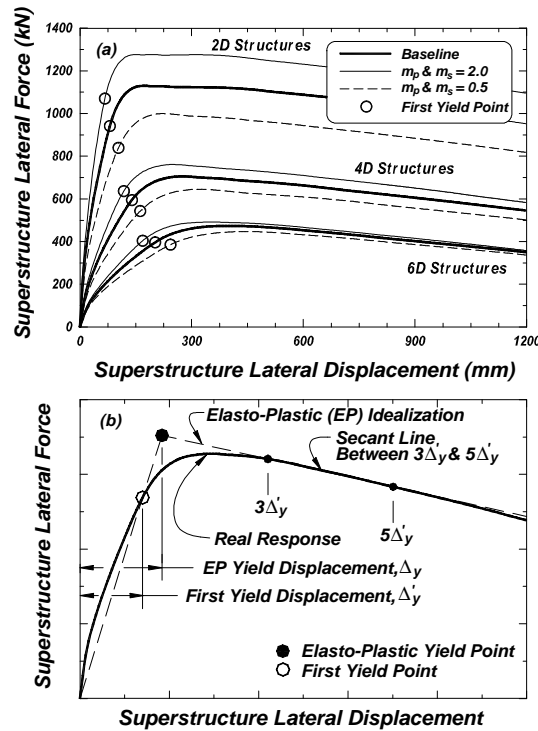


Figure 8. Pushover analyses of the superstructure supported on a 1.5-m diameter pile shaft with above-ground heights of 2D, 4D, and 6D.

- Effects of construction method on the soil properties and lateral stresses around the pile (e.g., driving vs. vibration vs. pre-drilling vs. CIDH). Construction effects are poorly understood and are not incorporated into current design practice.
- Generalized p-y relations may not capture the wide range of soil and loading conditions, including layering, loading rate, load history, cyclic degradation, two-dimensional loading, diameter effects, or other influences.
- Limitations in our modeling of the nonlinear behavior of reinforced concrete and other pile materials.

Curras et al. (2001) evaluated the potential variability in p-y parameters for a variety of soil conditions by re-analyzing a set of full-scale load tests. For each case, a baseline analysis was first performed using the computer program LPILE⁺ (Reese et al. 1997) with established p-y relations and common design procedures for selecting soil properties (i.e., without any knowledge of the actual load test response). Results were then compared to the recorded response. The analyses were then repeated to determine the factors by which the initial stiffness and ultimate strengths of the p-y relations must be scaled to accurately match the measured pile response. These independent scaling factors, m_p on the ultimate strength and m_s on the initial stiffness, may each be greater than, equal to, or less than one. The strength multipliers vary the ultimate strength but keep the stiffness constant, while the stiffness multipliers vary the initial stiffness while keeping the ultimate strength constant. In any one analysis, the m_p and m_s values are constant for all depths. The resulting scaling factors represented the combined effects of all influencing factors including model inadequacy and soil variability. From the set of load tests analyzed, the range of scaling factors provided some guidance on the inaccuracy and range of variability in the p-y representation for predicting the lateral loading response in design. The results suggested that the baseline analyses tended to underestimate lateral loading stiffness more often than they overestimated it. This is consistent with the p-y relations having a bias towards under-estimating lateral stiffness (i.e., conservative for most static loading problems) and/or the various correlations being biased towards underestimating soil strength and stiffness.

Scaling factors on p-y capacity (m_p) and stiffness (m_s) of 2.0, either up and down (m_p = m_s = 2.0 & m_p = m_s = 1/2), were chosen as being representative of reasonable ranges of variability. This range of scaling factors is reasonably consistent with results by other investigators (e.g., O'Neill and Murchison 1983, Murchison and O'Neill 1984, Ruiz 1986).

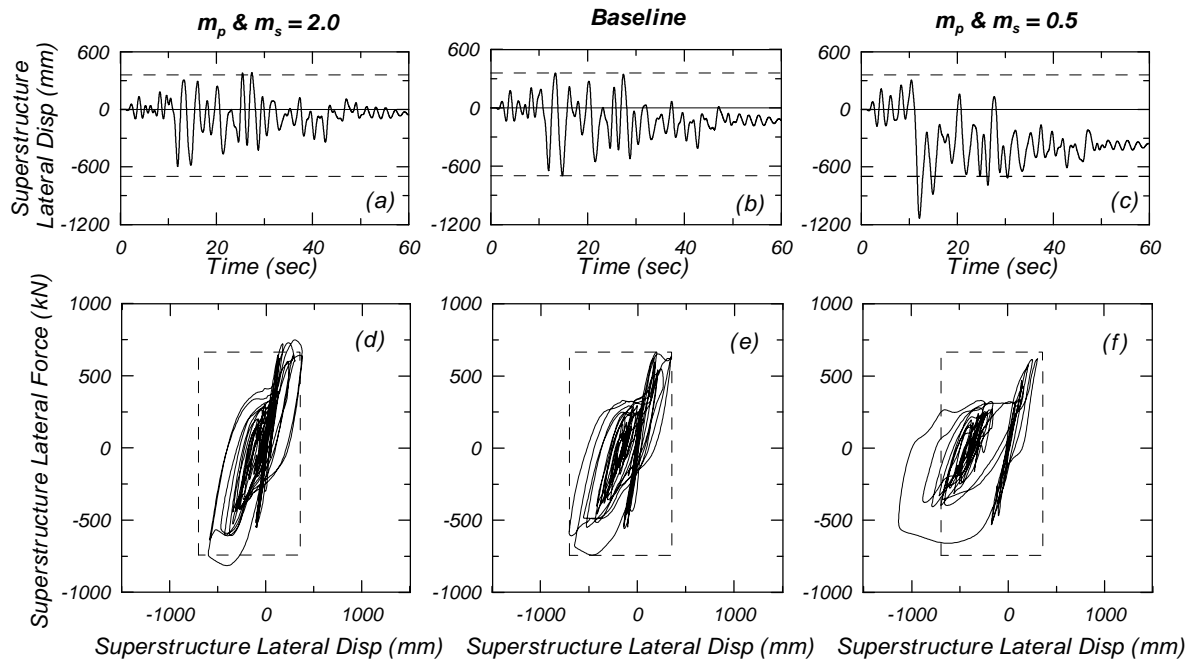


Figure 9. Superstructure response for the 1.5-m diameter pile, 4D above-ground structure, subjected to the Synthetic #2 outcrop motion with $a_{max}=0.7g$: Superstructure displacements for: (a) $m_p = m_s = 2.0$, (b) baseline, and (c) $m_p = m_s = 0.5$; Lateral force-displacement results for: (d) $m_p = m_s = 2.0$, (e) baseline, and (f) $m_p = m_s = 0.5$. Dashed lines envelope the baseline structure's response.

The effect of p-y stiffness and capacity on static and dynamic response was evaluated for the 1.5-m diameter pile shaft and a subset of ground motions. Results of the static pushover analyses for the 1.5-m diameter pile shaft are shown in Fig. 8(a) for above-ground heights of 2D, 4D, and 6D. The subset of outcrop motions consisted of the Synthetic #2 motion and the 1999 Yarımcı Petkim motion from Turkey, each scaled to peak accelerations (a_{max}) of 0.3, 0.5, and 0.7g for a total of 6 motions.

Elasto-plastic (EP) idealizations of the pushover results were obtained using the procedure in Fig. 8(b). The equivalent elastic stiffness is defined as the secant stiffness through the first yield point (i.e., the point at which any section first exceeds its yield moment). This equivalent elastic stiffness defines the corresponding equivalent elastic period of the structure (T_e). The EP yield point is defined by the intersection of the equivalent elastic and plastic secant lines as shown in Fig. 8(b). The post-elastic portion of the EP idealization is defined by extending a secant line through $3\Delta'_y$ and $5\Delta'_y$, which is nominally within current design ductilities for these types of structures (e.g., ATC-32 1996). The EP yield point identifies the EP yield displacement, Δ_y , and the EP lateral yield force, V_y .

Fig. 9 shows the effect of p-y parameter variations on the lateral displacement and force-displacement time histories of the 1.5-m diameter, 4D tall structure subjected to the Synthetic #2 outcrop motion with $a_{max} = 0.7g$. The baseline results shown earlier in Fig. 5 are repeated in parts (b) and (e) of Fig. 9, with the stiffer, stronger system ($m_p=m_s=2.0$) results to the left [parts (a) and (d)] and the softer, weaker system ($m_p=m_s=1/2$) results to the right [parts (c) and (f)]. Dashed lines that envelop the baseline structure's peak response are shown on parts (d)-(f) for comparison purposes. For these cases, it can be seen that the stiffer system had lower peak and residual displacements and the softer system had larger peak and residual displacements. The resulting global displacement ductility demands for these systems are $\mu_{\Delta} = 4.1$ for the baseline system, $\mu_{\Delta} = 4.1$ for the stiffer system (although the maximum displacement is lower than for the baseline system, the yield displacement is also lower), and $\mu_{\Delta} = 5.5$ for the softer system.

The changes in peak response quantities with the p-y parameter variation are shown in Fig. 10 for the 1.5-m diameter shaft (with above-ground heights of 2D, 4D, and 6D) and the Synthetic #2 and Turkey outcrop motions with a_{max} of 0.3, 0.5, and 0.7 g. These figures show the peak response quantity found in the soil parameter variation study versus the peak response for the corresponding baseline system, such that points falling on the

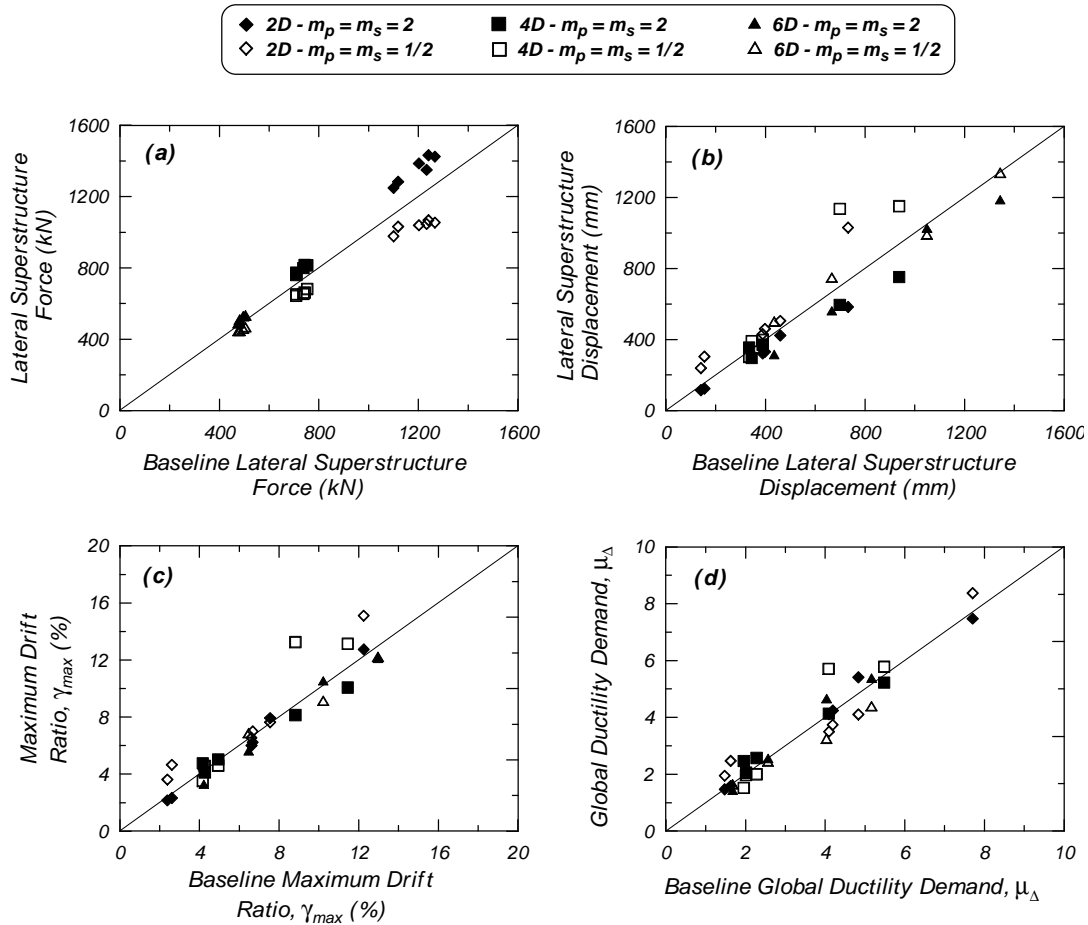


Figure 10. Effect of p-y parameter variations on peak responses for the 1.5-m diameter pile shaft: (a) superstructure lateral force, (b) superstructure lateral displacement, (c) superstructure drift ratio, and (d) global displacement ductility demand.

one-to-one line indicate no change in that response quantity. Part (a) shows the maximum lateral inertial forces, part (b) the maximum lateral displacements, part (c) the maximum superstructure drift ratio, and part (d) the maximum global displacement ductility demand at the superstructure. Solid data points are for the stiffer soil, open data points for the softer soil, and the various shapes indicate different above-ground structure heights.

The results for the 1.5-m diameter shaft in Fig. 10 are generally what would be expected. For instance, Fig. 10(a) shows that the maximum superstructure force increases in the stiffer systems and decreases in the softer systems, with the greatest difference being for the shortest structures and the least difference for the taller, more flexible structures. These trends are consistent with the results of the pushover analyses (Fig. 8), which defined the lateral strength capacity of the systems.

The maximum superstructure displacements in Fig. 10(b) show that the overall trend is for the stiffer systems to have smaller displacements and the softer systems to have larger displacements, although for most cases the differences are small. All together, 80% of the results are within $\pm 20\%$ of the baseline case. The maximum superstructure drift ratios in Fig. 10(c) follow the same trends as the displacements.

The global displacement ductility demands shown in Fig. 10(d) indicate that although the stiffer soil systems generally developed smaller displacements, their displacement ductility demand tended to be slightly greater. This is because the maximum displacements decreased by about 0 to 20% in most cases while the yield displacements decreased by about 10 to 20%. The net effect was a trend towards slightly larger displacement ductility demands. The converse statements are true for the softer soil systems – the maximum displacements were generally 0 to 20% larger (with a few cases of greater differences) while the yield displacements were 10 to

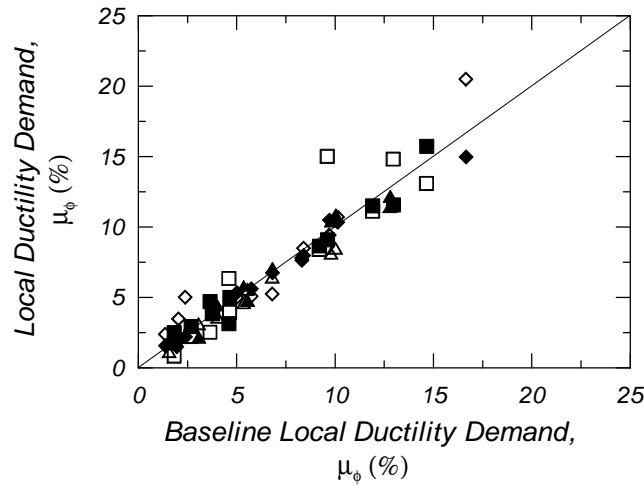
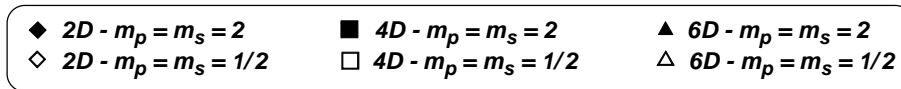


Figure 11. Effect of soil parameter variations on local ductility demand for the 1.5-m diameter pile shaft.

20% larger, resulting in a trend towards slightly smaller displacement ductility demands. Some softer soil systems did produce notable increases in displacement ductility demand, and these are the cases where the maximum displacements increased by more than 20%. Overall, about 80% of the μ_Δ results are within $\pm 20\%$ of their baseline value.

For these p-y parameter variations, the structures with an above-ground height of 2D showed many of the greatest percent differences in response quantities, which is consistent with the fact that the global strength and stiffness of these shorter structures are more affected by the lateral soil resistance. The 4D tall structures gave the greatest absolute differences in displacement demands, particularly for the Synthetic #2 outcrop motion. This observation is related to the fact that the displacement spectra for the ground surface motions produced by the Synthetic #2 motion change most rapidly in the period range corresponding to the 4D structures ($T_e \approx 1.3\text{-}2$ s).

The results in Fig. 10 illustrate some important observations. Assume a structure was designed for the baseline soil conditions, but in reality the soil response was closer to either the softer or stiffer p-y conditions. If the soil was softer, the maximum displacements would likely be larger than anticipated, but the global displacement ductility demand might be smaller. Conversely, if the soil is actually stiffer than expected, the displacements would likely be smaller, but the forces and global ductility demand might be larger. This suggests that for the structures and motions studied herein, a conservative design for the structural strength would assume stiffer soil conditions resulting in larger design values for global ductility and force demand. On the other hand, a conservative design to limit structural drift would assume softer soil conditions. These results illustrate the long-recognized point that neither softer or stiffer p-y parameters can be assumed to be conservative for seismic design, in contrast to the common expectation, usually derived from static design experiences, that assuming softer soil conditions is conservative.

Another important performance measure is the local curvature ductility demand (μ_ϕ) imposed on the structure by an earthquake, because damage to the pile (e.g. spalling of cover concrete, crack widths, potential for buckling or fracture of longitudinal reinforcement) is related to the local curvature ductility. The local ductility factor is defined as the maximum curvature (ϕ_{max}) divided by the elasto-plastic yield curvature (ϕ_y). In these cases, the maximum curvature was found by determining the maximum plastic rotation in the plastic hinge and dividing this rotation by the plastic hinge length (L_p). The plastic hinge length is assumed to follow the relation proposed by Chai and Hutchinson (1999), which gives $L_p=1.2D$ for the 2D-tall structures, $L_p=1.4D$ for the 4D-tall structures, and $L_p=1.6D$ for the 6D-tall structures.

Fig. 11 shows the effect of the p-y parameter variation on the local ductility demands for both the 1.5-m and 3.0-m diameter pile shafts with axial loads of $0.05 \cdot f'_c \cdot A_g$. These results indicate that the soil variation generally

had a smaller effect on the local ductility than it did on the other performance measures studied. For both pile shaft diameters, about one-half of the cases were within 10% of their baseline value and about two-thirds of the cases were within 15% of their baseline value (Fig. 11). The percent effect of the p-y parameter variations on the local ductility was generally greater at low levels of local ductility demand.

To understand this result, it is first necessary to examine the relation between local and global ductilities (μ_ϕ and μ_Δ , respectively). Softer p-y parameters resulted in larger local to global ductility demand ratios (μ_ϕ/μ_Δ) than for the baseline case, and stiffer p-y parameters resulted in smaller μ_ϕ/μ_Δ ratios. This trend is the same for both shaft diameters, although the 1.5-m diameter shaft had larger μ_ϕ/μ_Δ ratios than the 3-m diameter shaft. The predicted trend between soil conditions and μ_ϕ/μ_Δ ratios are consistent with experimental data, such as the full-scale load tests by Chai and Hutchinson (1999).

The typical effects that p-y parameter variations had on the structures' response can be summarized as follows. When softer p-y parameters were assumed:

- Yield displacement Δ_y increased
- Equivalent elastic period T_e increased
- Maximum displacement demand Δ_{max} increased
- Global displacement ductility μ_Δ demand decreased
- The ratio of local to global ductilities factors μ_ϕ/μ_Δ increased

As shown in Fig. 11, these factors can combine to cause the local curvature ductility demand μ_ϕ to be relatively unaffected.

ESTIMATING INELASTIC DISPLACEMENTS FOR DESIGN

Design methods commonly used to estimate inelastic displacement demands include R- μ -T (force reduction) and substitute structure methods. In this paper, inelastic demands from the dynamic FE analyses are compared to an R- μ -T method and to a mean spectral displacement method.

Force Reduction – Displacement Ductility – Period (R- μ -T) Relation

An important parameter in characterizing the inelastic response of a structure is the force reduction factor R, which is the ratio of the elastic lateral force demand to the lateral yield strength of the system. The elastic lateral force demand is obtained from the 5% damped elastic acceleration response spectra at the ground surface using the equivalent elastic period T_e of the system, as shown on Fig. 12(b). The displacement ductility factor is defined as $\mu_\Delta \equiv \Delta_{inelastic}/\Delta_y$, where $\Delta_y = EP$ yield displacement defined in Fig. 12(a) and $\Delta_{inelastic}$ = maximum displacement of the superstructure. Monotonic pushover analyses were performed to determine the parameters (V_y , Δ_y , T_e) defining the idealized elasto-plastic response for the different structures. The pushover analyses were repeated with P- Δ effects [e.g., Fig. 8(a)] and without P- Δ effects [e.g., Fig. 12(a)]. The inclusion of P- Δ effects caused softening of the pushover curve past the yield point, but did not significantly affect the idealized yield point (V_y , Δ_y) or the equivalent elastic period (T_e) for these structures.

A common approach for seismic design or analysis of structures assumes a basic relation between the force reduction factor R and the displacement ductility factor μ_Δ that characterizes the level of inelastic deformation in the structure. In this study, the relation between the force reduction factor R and the displacement ductility factor μ_Δ is plotted in Fig. 13 for bridge structures supported on a 3.0-m-diameter pile shaft. Note that the data in Fig. 13 included different periods ($T_e = 0.92$ to 3.79 s) and lateral strengths, which are primarily a result of varying the above-ground heights of the structure. As expected, the displacement ductility demand generally increases with increasing force reduction factor. For comparison purposes, the equal displacement assumption which implies $R = \mu_\Delta$, and the equal energy assumption which implies $R = \sqrt{2\mu_\Delta - 1}$, are also plotted on Fig. 13. For displacement ductility factor $\mu_\Delta > 3.0$, 86% of the analyses fall below the equal displacement principle and nearly all of these results are associated with near-fault or long-duration motions.

The general correlation between the force reduction factor R and displacement ductility factor μ_Δ often leads to the so-called R- μ -T relation for the prediction of inelastic displacements in structures. Although many R- μ -T

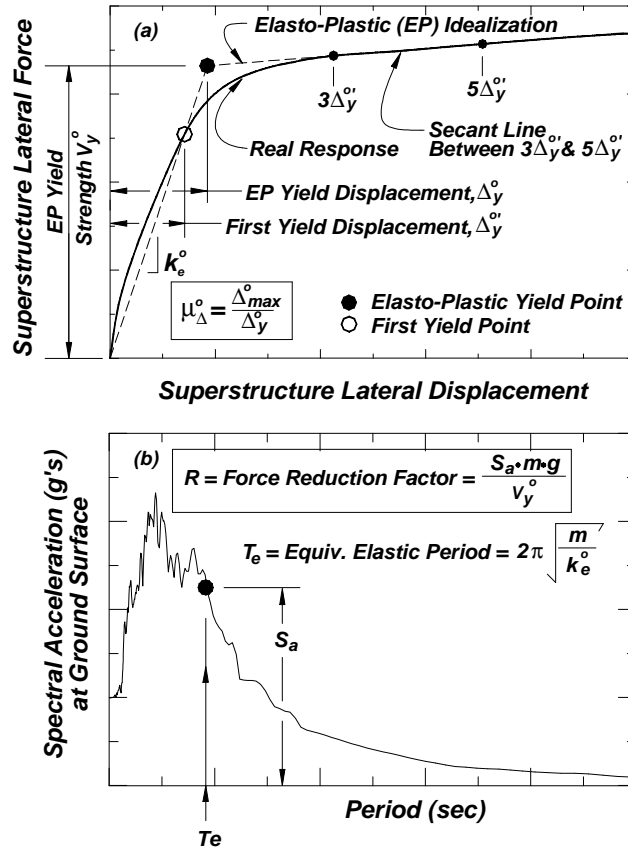


Figure 12. Definitions used in this study.

expressions exist in the literature, the analysis results for near-fault motions were compared to the expression by Vidic et al. (1994) with a slight modification. Vidic et al. assumed equal displacement in the long period range and a linear relation between the force reduction factor R and displacement ductility factor μ_{Δ} in the short period range. In equation form, their R - μ - T relation is given by:

$$(\mathbf{m}_{\Delta})_{Formula} = \begin{cases} (R-1) \cdot \frac{T_c}{T_e} + 1 & \text{for } T_e \leq T_c \\ R & \text{for } T_e > T_c \end{cases} \quad (1)$$

where T_c is the characteristic period of the ground motion. In this study, T_c is taken as the dominant pulse period T_p of these near-fault ground motions (Table 1) instead of that proposed by Vidic et al. (1994).

The applicability of the R - μ - T relation to bridge structures supported on extended pile shafts is studied through a comparison of the actual displacement ductility factor μ_{Δ} , as obtained from the FE analyses, with the displacement ductility factor $(\mu_{\Delta})_{Formula}$ calculated using Equation 1. The set of data in Fig. 13 with near-fault ground motions is plotted against the period ratio T_e/T_p in Fig. 14, in terms of the ratio of displacement ductility factors C_{μ} , where:

$$C_{\mu} = \frac{\mathbf{m}_{\Delta}}{(\mathbf{m}_{\Delta})_{Formula}} \quad (2)$$

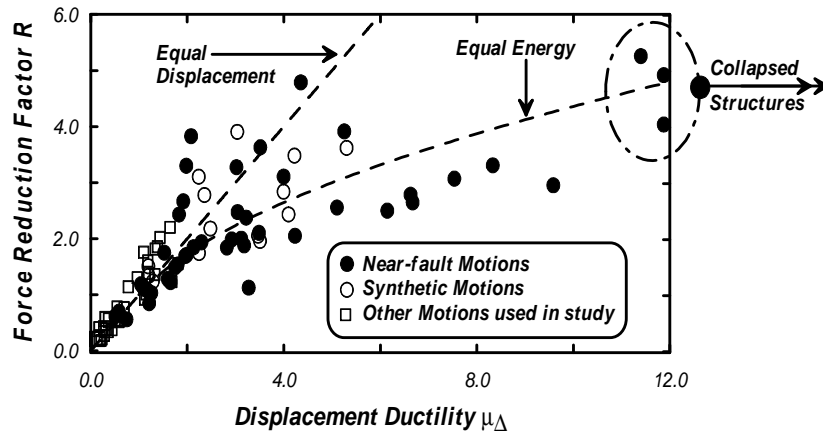


Figure 13. R- m relation for structures supported on extended pile shafts with a 3.0-m diameter.

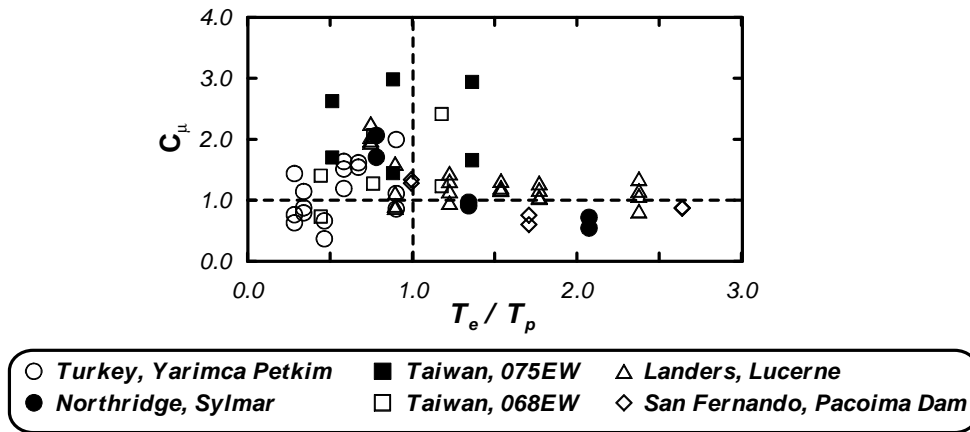


Figure 14. Ductility ratio C_{μ} versus period ratio T_e/T_p for structures supported on 1.5-m and 3.0-m diameter pile shafts and subjected to near-fault motions.

The data in Fig. 14 correspond to the ratio of displacement ductility factors C_{μ} with P- Δ effects; Results without P- Δ effects are very similar and lead to the same general observations. For $T_e/T_p \leq 1.0$, 70% of the dynamic analysis cases were underestimated using Equation 1 (i.e. $C_{\mu} > 1.0$). The mean of these analyses with $T_e/T_p \leq 1.0$ is $C_{\mu} = 1.43$, with a coefficient of variation (COV) of 41%. When T_e/T_p is less than 1.0, yielding of the structure causes its secant period to lengthen and become closer to the dominant pulse period of the ground motion. Conversely, if the ratio T_e/T_p is greater than 1.0, yielding of the structure causes its secant period to lengthen and move further away from the dominant pulse period of the ground motion. For the data with $T_e/T_p \geq 1.0$, the ratio of displacement ductility factors C_{μ} is closer to 1.0 except for three cases where $C_{\mu} > 1.5$ developed during the Taiwan motions with peak outcrop accelerations of 0.3 and 0.5 g. These motions had a wide long-period band of strong spectral ordinates that descended fairly slowly in the spectra. Excluding these three data points, the mean of the data where $T_e/T_p > 1.0$ was $C_{\mu} = 1.05$ with a COV=23%, suggesting that the equal displacement assumption is reasonable for these long-period structures, provided the elastic period of the structure is greater than the predominant period of the pulse.

The C_{μ} versus T_e/T_p results in Fig. 14 show that ductility demands from near-fault ground motions are generally underestimated by Equation 1 if the elastic period of the structure is less than the ground motion's dominant pulse period. The scatter in the analysis results is understandable given the many complicating factors, including the facts that the ratio T_e/T_p provides no information on the strength of the pulse in the ground motion and that it is difficult to define the dominant pulse period T_p in practice.

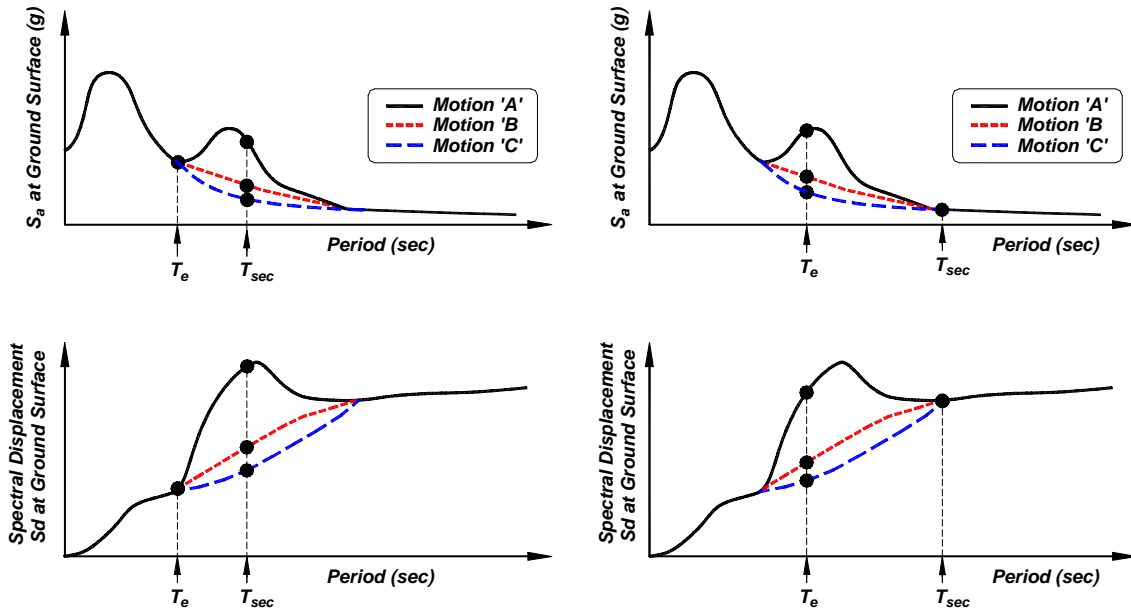


Figure 15. Schematic illustrating the difficulty in estimating demands from near-fault motions using a single spectral period.

Mean Spectral Displacement Method

R- μ -T relations appear to have limited accuracy in predicting the effects that long-period pulses have on these types of structures. One possible reason is that they generally use a single response spectra ordinate as an input to the relation; e.g., The equivalent elastic period T_e of the structure and an elastic response spectrum are used to estimate displacement demand (or force demand through the force reduction factor). A basic limitation in using a single period T to estimate displacement demands from spectra for ground motions with a strong long-period pulse is illustrated in Fig. 15. In the example on the left side of Fig. 15, the three motions have identical elastic response spectral values for the given elastic structural period (T_e), but have very different spectral values at longer periods (such as might be introduced by a near-fault pulse). Inelastic deformations will degrade the structural stiffness and lengthen the effective period of the system. The secant stiffness at the peak superstructure displacement can be used to define a secant period T_{sec} that represents the longest effective period of the system. The three motions on the left side of Fig. 15 have very different spectral values at T_{sec} despite having the same value at T_e . The example on the right side of Fig. 15 illustrates the same concept, except that the three spectra have very different spectral values at T_e and the same spectral value at T_{sec} . From these schematic examples, it seems reasonable to expect that the structure's inelastic displacement may be better related to the spectral content between T_e and T_{sec} , and not just to the spectral value at any single value of T .

An alternative approach for the prediction of inelastic displacements is explored herein. This approach uses the mean spectral displacement between two periods that are considered most relevant to the structure's response. In equation form, the inelastic displacement is calculated from the elastic displacement spectrum using:

$$\Delta_{mean} = \frac{1}{T_2 - T_1} \int_{T_1}^{T_2} S_d^e(T) \cdot dT \quad (3)$$

where $S_d^e(T)$ = elastic displacement spectrum, and T_1 and T_2 define the period interval considered most important to the structure. Note that the damping ratio for the elastic displacement spectra was taken as 5%, and was not adjusted for the hysteretic yielding of the structure. Several possibilities for defining the "period interval" for the integral in Equation 3 are discussed below. Each definition of the period interval was evaluated by its effect on the ability of Equation 3 to predict the dynamic analysis results. As was previously suggested and

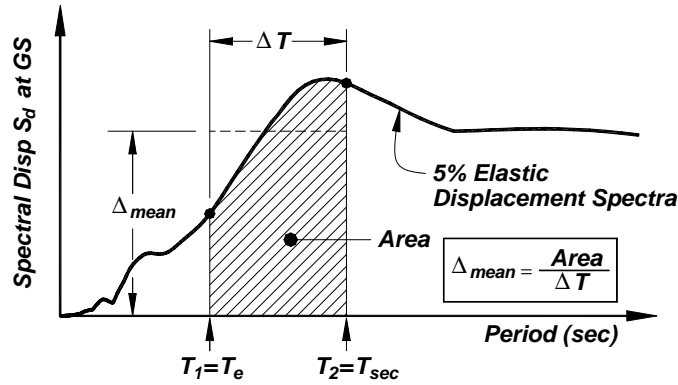


Figure 16. Mean spectral displacement method using the elastic displacement spectra at the ground surface and a period interval between T_1 and T_2 .

will be shown below, a promising choice for defining the period interval is to assume $T_1 = T_e$ = elastic period of the structure, and $T_2 = T_{sec}$ = secant period of the structure defined using the maximum inelastic displacement of the structure. The mean spectral displacement approach is shown schematically in Fig. 16 for the case where T_e and T_{sec} are used to define the period interval for Equation 3.

The relative merits of this approach were evaluated in Fig. 17 by comparing several different choices for the period interval. The cases shown in Fig. 17 are for structures supported on 3.0-m diameter pile shafts with axial loads of $0.05 \cdot f_c' A_g$ and including P- Δ effects (similar results were obtained without P- Δ effects). These analyses are the same as those shown in Fig. 13. In all cases, displacement ratios C_Δ were used to compare the predictions by Equation 3 to the dynamic analysis results, as:

$$C_\Delta = \frac{\Delta_{inelastic}}{\Delta_{mean}} \quad (4)$$

where $\Delta_{inelastic}$ is the maximum (inelastic) displacement from the dynamic analysis, and Δ_{mean} is the mean spectral displacement demand as determined by Equation 3. It follows that C_Δ values less than 1.0 indicate that Equation 3 produced a conservative (high) estimate of inelastic displacement. Fig. 17(a) shows a case where the two periods are both taken as T_e (i.e., as if only one period was used). In this case, a displacement ratio $C_\Delta=1.0$ would correspond to the equal displacement assumption.

Figs. 17(b) and 17(c) show cases where the two periods are both taken as T_{sec} (i.e., as if only one period was used). For Fig. 17(b), T_{sec} was defined at the peak inelastic displacement from the dynamic analysis, which assumes that the correct inelastic displacement is known. While this is clearly never the case, this approach was nonetheless used as a means of conceptually evaluating the method. For Fig. 17(c), T_{sec} was defined at the peak displacement predicted by the intersection of the nonlinear pushover response and the elastic displacement spectra, as illustrated in Fig. 18. There is a slight loss of accuracy in going from Fig. 17(b) to 17(c), which is understandable given that the approach in 17(b) assumes the correct inelastic displacement is known.

Figs. 17(d) and 17(e) show cases where the period interval is defined by $T_1=T_e$ and $T_2=T_{sec}$. For Fig. 17(d), T_{sec} was defined at the peak inelastic displacement from the dynamic analysis, while for Fig. 17(e), T_{sec} was defined at the peak displacement predicted by the intersection of the nonlinear static pushover response and the elastic displacement spectra (as illustrated in Fig. 18). There is a slight loss of accuracy going from Fig. 17(d) to 17(e), as was seen from 17(b) to 17(c), due to the fact that 17(d) assumes the correct inelastic displacement is known. Regardless of how T_{sec} was defined, the use of a mean spectral displacement between $T_1=T_e$ and $T_2=T_{sec}$ resulted in a smaller standard error than was obtained using only a single period [i.e., using only the elastic period ($T_1=T_2=T_e$) or only the secant period ($T_1=T_2=T_{sec}$)]. This can be seen by comparing either Figs. 17(a), 17(b), and 17(d), or Figs. 17(a), 17(c), and 17(e). In addition, the use of a mean spectral displacement resulted in a C_Δ that had virtually no dependence on μ_Δ .

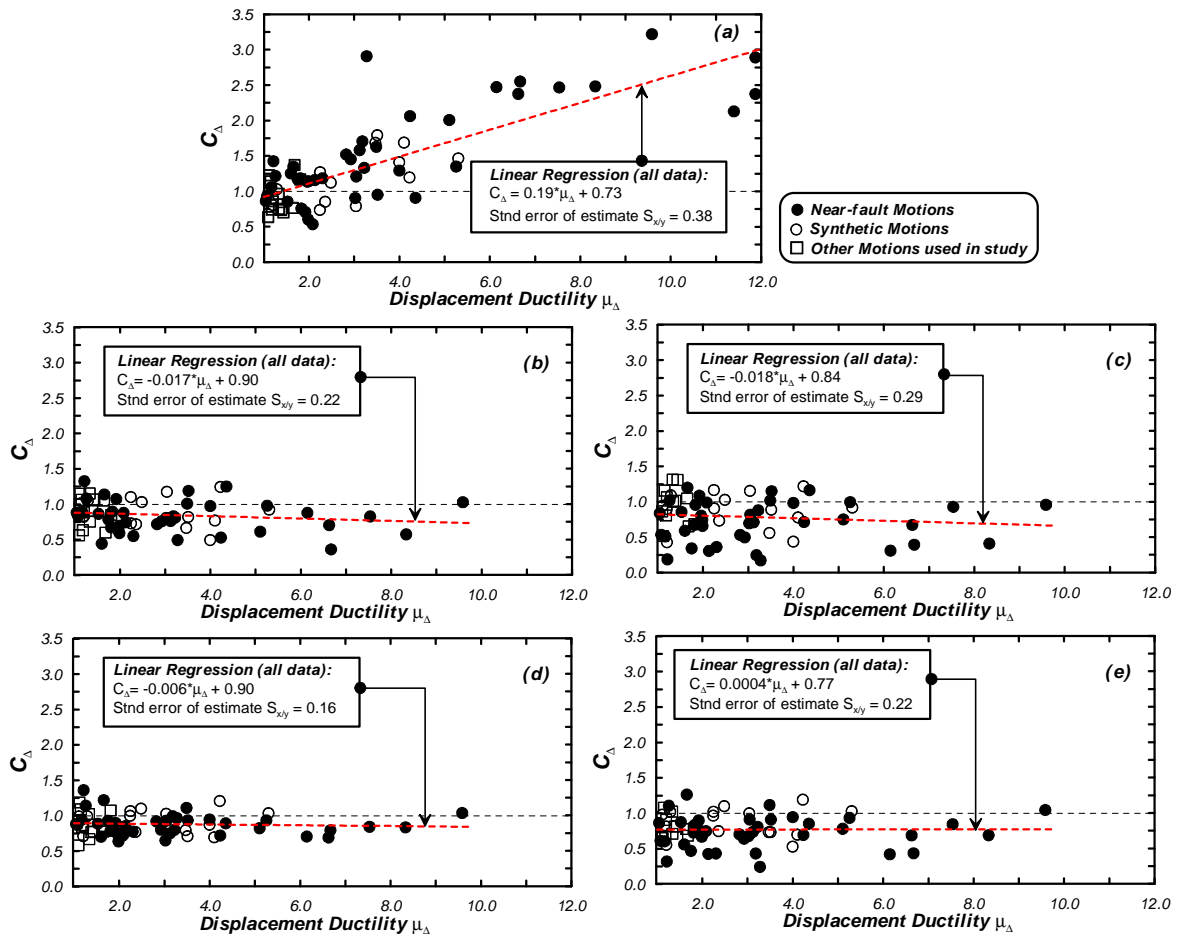


Figure 17. Displacement ratios $C_D (= D_{inelastic}/D_{mean})$ as a function of m_D for 3.0-m diameter pile shafts with P-D effects;
 (a) C_D based on $T_1=T_2=T_e$,
 (b) C_D based on $T_1=T_2=T_{sec}$ at peak m_D from dynamic analysis,
 (c) C_D based on $T_1=T_2=T_{sec}$ at intersection of pushover and elastic displacement spectra,
 (d) C_D based on $T_1=T_e$ and $T_2=T_{sec}$ at peak m_D from dynamic analysis, and
 (e) C_D based on $T_1=T_e$ and $T_2=T_{sec}$ at intersection of pushover and elastic displacement spectra.

The results in Fig. 17 represent an initial evaluation of the conceptual merits of using the mean spectral displacement method (Equation 3), and as such suggest that the method has promise for reducing uncertainty in predicting inelastic displacements for these types of structures during near-fault motions. Additional efforts are underway to evaluate the method over a broader range of structural periods and ground motions, and explore refinements that might improve its accuracy. For example, some immediate refinements may be to use the secant period T_{sec} that corresponds to the inelastic displacement predicted by Equation 3 (along with T_e for defining the period interval), or to evaluate some simple weighting functions for integrating the area under the elastic displacement spectra.

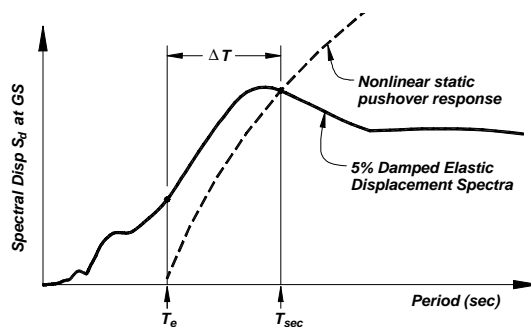


Figure 18. Estimating the secant period T_{sec} of a structure by the intersection of its nonlinear pushover response and the elastic displacement spectra.

SUMMARY AND CONCLUSIONS

The seismic response of bridge and viaduct structures supported on large-diameter extended CIDH pile shafts was evaluated using nonlinear static and nonlinear dynamic analysis methods. Results presented herein focussed on the effects that near-fault ground motions and variable lateral soil resistance have on performance. The correlation between maximum and residual drift ratios from the dynamic analyses indicates that strong near-fault motions may result in large permanent displacements in the structure, rendering the structure unusable or even unsafe. The importance of P- Δ effects for structures that experience large drift ratios was demonstrated, while additional work on quantifying the effects over the full range of responses continues.

The effects of p-y parameter variations on the static pushover and dynamic response were evaluated. Scaling the p-y capacity (m_p) and stiffness (m_s) by factors of $m_p = m_s = 2.0$ and $m_p = m_s = 1/2$ was studied for a subset of motions and structures. Stiffening the p-y parameters generally resulted in a larger lateral yield force, smaller lateral yield displacement, smaller equivalent elastic period, smaller displacement demand, slightly larger global displacement ductility demand, and relatively similar local curvature ductility demand. Softening the p-y parameters generally had the opposite effects. These results should not be generalized to other classes of structures, however, because there are clearly situations where variations in the substructure stiffness can have a much more significant effect on system performance.

Inelastic displacements predicted using an R- μ -T relation were compared to the displacement demands calculated by the dynamic analyses. The equal displacement assumption, as implied by the R- μ -T relation in the long-period range, appears to be reasonable for near-fault motions provided the elastic period of the structure is longer than the period of the pulse (if present). In the shorter-period range, however, the R- μ -T relation in Equation 1 underestimated the inelastic displacements. An adjustment to the R- μ -T relation for the effects of long-period pulses was explored, where the adjustment depended on the T_e/T_p ratio (T_e = equivalent elastic period of structure, T_p = dominant pulse period). The resulting relation still had a large coefficient of variation, which is understandable given that the T_e/T_p ratio provides insufficient information regarding the pulse characteristics relative to the other components of the ground motion.

An alternative design method for prediction of inelastic displacements was explored that uses the mean elastic spectral displacement (for 5% damping) between two periods that bracket the range of motions most important to the structure. When these two periods are taken as the elastic period (T_e) and the secant period at peak displacement demand (T_{sec}), the results showed a substantial reduction in the standard error of the estimate. This improvement in the accuracy of predicting inelastic displacements, given a site-specific displacement spectrum of a near-fault ground motion, indicates that this approach has promise and thus it is being evaluated in greater detail.

Acknowledgements

The Pacific Earthquake Engineering Research Center funded this research under grant 2081999. T. C. Hutchinson was supported by a fellowship from the Earthquake Engineering Research Institute (EERI). R. L.

Taylor and F. Filippou generously shared their computer codes and provided valuable interaction throughout this study. Norm Abrahamson provided some of the processed ground motions. The above support and assistance is greatly appreciated.

References

- Applied Technology Council (1996). "Improved Seismic Design Criteria for California Bridges: Provisional Recommendations ATC-32." June.
- Baez, J.I. and Miranda, E. (2000). "Amplification factors to estimate inelastic displacement demands for the design of structures in the near field," Proc. 12th World Conf. on Earthquake Engrg., Auckland, NZ.
- Bertero, V.V., Mahin, S.A. and Herrera, R.A. (1978). "Aseismic design implications of near-fault san fernando earthquake records." Earthquake Eng. and Struct. Dynamics, Vol. 6, pp. 31-42.
- Boore, D.M. (1973). "The effect of simple topography on seismic waves: implications for the accelerations recorded at Pacoima Dam, San Fernando Valley, California." Bull. Seism. Soc. Am. 63, pp.1603-1609.
- Boulanger, R. W., Curras, C. J., Kutter, B. L., Wilson, D. W., & Abghari, A. (1999). "Seismic soil-pile-structure interaction experiments and analyses." J. Geotech. and Geoenv. Engrg., ASCE 125(9): 750-759.
- Chai, Y. H. & Hutchinson, T. C. (1999). Flexural strength and ductility of reinforced concrete bridge piles. Report UCD-STR-99-2, University of California, Davis.
- Curras, C. J., Hutchinson, T. C., Boulanger, R. W., Chai, Y.-H., and Idriss, I. M. (2001). "Lateral loading & seismic response of CIDH pile supported bridge structures," Proceedings, Geo-Odyssey, Geotechnical Special Publication, ASCE (in-press).
- Curras, C. J. (2000). Seismic soil-pile-structure interaction for bridge and viaduct structures. Ph.D. thesis, University of California, Davis.
- EPRI (1993). Guidelines for determining design basis ground motions, Volume 3. TR-102293, Electric Power Research Institute, Palo Alto, California.
- Filippou, F. C. (1999). FEDEAS: Finite Elements for Design, Evaluation, & Analysis of Structures. On-line manual: <http://www.ce.berkeley.edu/~filippou/Research/>, Univ. of California, Berkeley, CA.
- Idriss, I. M., & Sun, J. (1991). User manual for SHAKE91. Center for Geotechnical Modeling, Dept. of Civil and Envir. Engineering, University of California, Davis, CA.
- Kent, D.C., and Park, R. (1971). "Flexural members with confined concrete." Journal of Structures Division, ASCE, 97(ST7): 1964-1990.
- MacRae, G.A. and Kawashima, K. (1997). "Post-earthquake residual displacements of bilinear oscillators," Earthquake Engineering and Structural Dynamics, Vol. 26, pp. 701-716.
- Mahin, S.A. and Hachem, M. (1998). "Response of simple bridge structures to near-fault ground motions." 5th Caltrans Seismic Research Workshop, June 17-18, Sacramento, CA.
- Menegotto, M. and Pinto P.E. (1973). "Methods of analysis for cyclically loaded reinforced concrete plane frames including changes in geometry and nonelastic behavior of elements under combined normal force and bending." IABSE Symposium on resistance and ultimate deformability of structures acted on by well-defined repeated loads, Final Report, Lisbon.
- Murchison, J. M., & O'Neill, M. W. (1984). "An evaluation of p-y relationships in cohesionless soils." Analysis and design of pile foundations, J. R. Meyer, ed., ASCE, New York, 174-191.
- O'Neill, M. W., & Murchison, J.M. (1983). "An Evaluation of p-y relationships in Sands." API Report PRAC 82-41-1.
- Page, R.A., Boore, D.M., Joyner, W.B., and Coulter, H.W. (1972). Ground motion values for use in the seismic design of the Trans-Alaska pipeline system. U.S.G.S. Circular 672, 23 pp.
- Reese, L. C., Wang, S.T., Arréllaga, J. A., & Hendrix, J. (1997). LPILE Plus Version 3.0 – A Program for the Analysis of Piles and Drilled Shafts Under Lateral Loads. Ensoft, Inc. Austin, Texas.
- Ruiz, S. E. (1986). "Uncertainty about p-y curves for piles in soft clays." Journal of Geotechnical Engineering, 112(6): 594-607.
- Schnabel, P. B., Lysmer, J. & Seed, H. B. (1972). SHAKE: a computer program for earthquake response analysis of horizontally layered sites. UCB/EERC-72/12, EERC, Univ. of California, Berkeley, 102 p.
- Taylor, R. L. (1998). FEAP – A finite element analysis program. Department of Civil and Environmental Engineering, University of California, Berkeley.
- Trifunac, M.D. and Brady, A.G. (1975). "A study on the duration of strong earthquake ground motion." Bulletin of the Seismological Society of America, Vol. 65, No. 3, pp. 581-626.
- Vidic, T., Fajfar, P. and Fischinger, M. (1994). "Consistent inelastic design spectra: strength and displacement." Earthquake Engineering and Structural Dynamics, Vol. 23, pp. 507-521.